Mass anomalous dimension in sextet QCD

Thomas DeGrand

Department of Physics, University of Colorado, Boulder, CO 80309, USA

Yigal Shamir and Benjamin Svetitsky

Raymond and Beverly Sackler School of Physics and Astronomy, Tel Aviv University, 69978 Tel Aviv, Israel

We extend our previous study of the SU(3) gauge theory with $N_f = 2$ flavors of fermions in the sextet representation of color. Our tool is the Schrödinger functional method. By changing the lattice action, we push the bulk transition of the lattice theory to stronger couplings and thus reveal the beta function and the mass anomalous dimension γ_m over a wider range of coupling, out to $g^2 \simeq 11$. Our results are consistent with an infrared fixed point, but walking is not ruled out. Our main result is that γ_m never exceeds 0.45, making the model unsuitable for walking technicolor. We use a novel method of extrapolation to the large-volume/continuum limit, tailored to near-conformal theories.

PACS numbers: 11.15.Ha, 11.10.Hi, 12.60.Nz

I. INTRODUCTION

For some time we have been studying SU(N) gauge theories with fermions in the symmetric two-index representation of color [1–8]. These are among the theories that have been proposed [9–11] as candidate models for walking technicolor [12–15]. Here we present our most recent work on the SU(3) gauge theory with $N_f = 2$ flavors of fermions in the sextet representation.

A technicolor theory must supply Goldstone bosons in order to generate masses for the weak vector bosons. To that end, the theory must break chiral symmetry spontaneously. In order to generate quark and lepton masses as well while avoiding large effects of flavor-changing neutral currents, one demands the additional property of *walking*. Here a large separation between the technicolor scale Λ_{TC} and the "extended" technicolor scale Λ_{ETC} is attained by having a near-zero of the beta function; the running coupling stalls for many decades in energy before chiral symmetry breaking sets in at large distances. Furthermore, the effect of the large ratio $\Lambda_{ETC}/\Lambda_{TC}$ on the technifermion condensate has to be enhanced by a large anomalous dimension γ_m of the mass operator $\bar{\psi}\psi$. Current estimates [16] require $\gamma_m \simeq 1$. In fact $\gamma_m = 1$ emerges from analyses based on the gap equation for walking technicolor [13, 14] (see also [17]).

Since the beta function and γ_m are the important ingredients of walking technicolor, our work has focused on measuring them. We do this using Schrödinger-functional (SF) techniques [18–23], which are a lattice implementation of the background-field method. For other instances of the Schrödinger functional applied to technicolor candidates, see [24–30].

Our first effort [1] used Wilson's fermion action with an added clover term [31] to reduce $O(a)$ effects, and was limited to lattices of linear size $L = 4a$, $6a$, and $8a$. The result was a discrete beta function that appeared to cross zero at a renormalized coupling $g^2 \simeq 2.0$, indicating an infrared fixed point (IRFP). An IRFP indicates conformal physics at large distances, the antithesis of confinement. Intending to understand (and reduce) discretization effects, we then [4] went to larger lattices, $L/a = 6$, 8, 12, 16, and began using hypercubic smearing—fat links [32, 33]—in the fermion action. This work showed that the IRFP of Ref. [1] was but a lattice artifact. Thanks to its numerical stability, the fat-link action also enabled us to simulate at stronger couplings, out to $g^2 \simeq 4.6$, corresponding to a bare coupling $\beta = 4.4$. At stronger bare couplings we encountered a phase transition that makes it impossible to tune the hopping parameter κ so as to make the quark mass zero. The result of Ref. [4], then, is a beta function that is smaller in magnitude than the two-loop result but that does not cross zero in the accessible range of couplings.

In Ref. [4] we also calculated the anomalous dimension γ_m according to the method of [27, 34–36]. We found that γ_m first follows the one-loop curve but its rise slows at strong couplings so that $\gamma_m \lesssim 0.6$ in the range of couplings that we could reach.

In our work on the SU(4) gauge theory with two-index (decuplet) fermions [7, 8], we encountered the same phase transition that prevents simulation of the massless theory. We found that augmenting the pure-gauge part of the action with a new fat-plaquette term can move this transition to stronger bare coupling and stronger renormalized coupling as well. In the present paper, we present the result of applying this strategy to the SU(3) theory. The new action enables us to reach $g^2 \simeq 11$, which is in the vicinity of the zero of the two-loop beta function, discussed by Caswell [37] and by Banks and Zaks [38].

While at first glance our calculated beta function crosses zero near the two-loop zero, further analysis

shows that this result is not stable under extrapolation to the continuum limit. It is quite possible that the beta function of this theory approaches zero in the range of coupling that we can study, and then veers away from zero at yet stronger couplings—much as envisioned in scenarios of walking.

Whether the beta function crosses zero or no, we find, in agreement with our earlier work, that the anomalous dimension has left the one-loop curve and leveled off. The limit we set at our strongest coupling is $\gamma_m \lesssim 0.45$. Our earlier work, based on the pure plaquette gauge action, quoted values approaching 0.6, but this was without attempting to remove lattice artifacts. We report here an analysis of lattice artifacts that allows smooth extrapolation to the continuum limit. The results for both actions move downwards and the error bars grow under extrapolation. As a result, the results for the two actions are not in violent disagreement. The small value of γ_m near the (real or approximate) fixed point spells trouble for any use of the present theory as walking technicolor.

The plan of this paper is as follows. In Sec. II we present the improved lattice action, which is the only difference in the simulation method between this paper and Ref. [4]. For other details of our simulations we refer the reader to Ref. [4]. We also briefly discuss the ensembles we generated, and how we deal with the autocorrelations of our observables. We proceed in Sec. III to present our results for the running coupling and the beta function. We re-analyze the data of Ref. [4] according to the lights of our later paper on the SU(2) theory [6], where we learned to take advantage of the slow running in order to make maximum use of the several lattice sizes in play. Naturally, we add in the results of the new simulations obtained with the augmented gauge action. Our first results show an apparent zero in the beta function; this will not survive our analysis of discretization error later in the paper. Section IV contains our numerical results for the mass anomalous dimension γ_m. We study the finite-lattice corrections to both γ_m and the beta function in Sec. V. The former reaches a smooth continuum limit, albeit with larger error bars than those of the raw results of Sec. IV; the latter is not so well-behaved. In Sec. VI we summarize our results and place them in the context of other work. In the appendix we examine the fermion contribution to the one-loop SF coupling and explain that it does not provide any guidance for the range of couplings and volumes that we study.

II. LATTICE ACTION AND ENSEMBLES

Our action contains a fermion term and two pure gauge terms. The fermion term $\bar{\psi} D_F \psi$ is the conventional Wilson action, supplemented by a clover term [31] with coefficient $c_{\rm SW} = 1$ [39]. The gauge links in the fermion action are fat link variables $V_\mu(x)$. The fat links are the normalized hypercubic (nHYP) links of Ref. [32], where for each link (x, μ) one takes the weighted average $V_\mu(x)$ of links in neighboring hypercubes with weights $\alpha_1 = 0.75$, $\alpha_2 = 0.6$, $\alpha_3 = 0.3$, reunitarized and subsequently promoted to the sextet representation.

The gauge action is

$$\begin{aligned} S_G &= -\frac{\beta}{2N} \sum_{\mu\neq\nu} \mathrm{Re}\,\mathrm{Tr}\, U_\mu(x) U_\nu(x+\hat{\mu}) U_\mu^\dagger(x+\hat{\nu}) U_\nu^\dagger(x) \\ &\quad -\frac{\beta_6}{2d_f} \sum_{\mu\neq\nu} \mathrm{Re}\,\mathrm{Tr}\, V_\mu(x) V_\nu(x+\hat{\mu}) V_\mu^\dagger(x+\hat{\nu}) V_\nu^\dagger(x), \end{aligned} \tag{1}$$

wherein the first term is the usual sum of plaquettes of fundamental thin link variables, while the second term contains plaquettes made of fat links in the sextet representation as in the fermion action. $N = 3$ is the number of colors while $d_f = 6$ is the dimension of the fermion representation, here the sextet. The weak-coupling expansion of S_G gives the effective bare coupling [7],

$$\frac{1}{g_0^2} = \frac{\beta}{2N} + \frac{T_6 \beta_6}{6}\,, \tag{2}$$

where $T_6 = 5/2$ is the group trace in the fermions' representation.[1]

As before, we employ the hybrid Monte Carlo (HMC) algorithm in our simulations. The molecular dynamics integration is accelerated with an additional heavy pseudo-fermion field as suggested by Hasenbusch [40], multiple time scales [41], and a second-order Omelyan integrator [42]. We determined the critical hopping parameter $\kappa_c = \kappa_c(\beta)$ by setting to zero the quark mass, as defined by the unimproved axial Ward identity on lattices of size $L = 12a$.

Without a systematic search, we found that choosing $\beta_6 = +0.5$ removes the strong-coupling phase transition so that we can run at bare couplings down to $\beta = 2.0$; at smaller β the acceptance deteriorates rapidly, especially for larger volumes, so that we did not go far enough to find out if and where the strong-coupling transition turns up. At $\beta = 2.0$, the running coupling for $L = 6$ turns out to be $g^2 \simeq 11$. This is close to the two-loop Banks–Zaks zero at $g^2 = \frac{13}{194}(16\pi^2) \simeq 10.6$. We list in Table I the values of (β, κ_c) and the number of trajectories run at each volume, along with the length of the trajectories and the acceptance. Poor acceptance forced us to shorten the trajectory length in many cases from the usual value of 1.

The observables we measure are the (inverse) SF running coupling, $1/g^2$, and the pseudoscalar renormalization factor, Z_P. (We measure Z_P on the same configurations used to determine $1/g^2$.) Both of them turn out to have long autocorrelation times. We monitored and controlled this problem by running 4 or 8 streams in

[1] We presented a test of weak-coupling universality in our paper on the SU(4) theory [8].

TABLE I: $\beta_6 = 0.5$ ensembles generated at the bare couplings (β, κ_c) for the lattice sizes L used in this study. Listed are the total number of trajectories for all streams at given (β, L), the trajectory length, and the HMC acceptance.

β	κ_c	L/a	trajectories (thousands)	trajectory length	acceptance
3.5	0.13349	6	74.8	1.0	0.93
		8	15.5	0.5	0.97
		10	8.0	1.0	0.75
		12	37.0	0.5	0.88
2.5	0.13991	6	8.8	1.0	0.61
		8	14.3	1.0	0.43
		10	20.4	0.5	0.75
		12	35.6	0.5	0.50
		14	11.6	0.5	0.61
		16	17.1	0.5	0.48
2.0	0.14273	6	17.2	1.0	0.65
		8	14.2	0.5	0.61
		10	12.0	0.5	0.67
		12	13.4	0.5	0.48
		16	29.6	0.4	0.38

TABLE II: $\beta_6 = 0$ ensembles generated at the new lattice sizes $L = 10a$ and $14a$, which we add to the ensembles listed in Ref. [4]. Columns as in Table I.

β	κ_c	L/a	trajectories (thousands)	trajectory length	acceptance
4.8	0.13173	10	9	1.0	0.95
4.4	0.13510	10	16	1.0	0.80
		14	12	0.5	0.85

parallel at each β and L. After analyzing each stream separately, we fit the results of the streams together to a constant. We demanded that the χ^2/dof of the constant fit not exceed 6/3 for 4 streams, or 10/7 for 8 streams. For the largest volume $L = 16a$ at the strongest coupling $\beta = 2.0$, we were not able to overcome the autocorrelations in $1/g^2$ even with nearly 30,000 trajectories. We therefore omit this point from the analysis of the running coupling. The autocorrelations in Z_P, on the other hand, did allow a consistent determination, and thus we keep this point in the analysis of the mass anomalous dimension.

In this paper we present our new results, obtained with $\beta_6 = 0.5$, alongside the $\beta_6 = 0$ results presented in our earlier paper [4]. For the more extensive study of discretization error in Sec. V, we supplemented the data of Ref. [4] with simulations on new lattice sizes $L = 10a, 14a$ at two values of β in strong coupling, as shown in Table II.

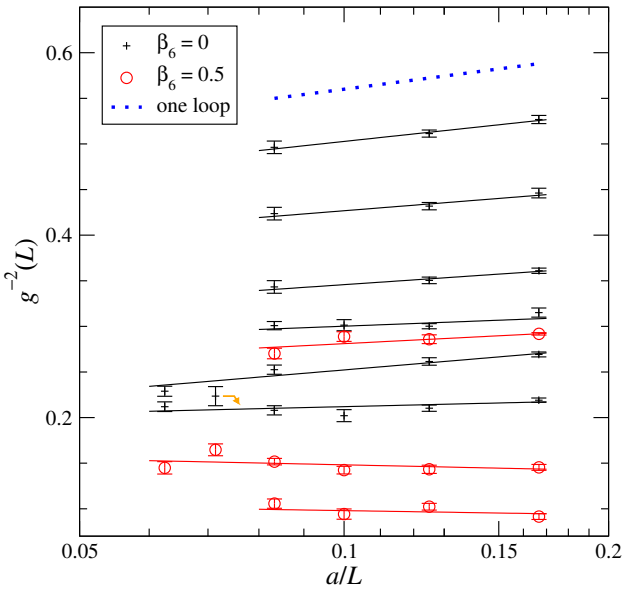

FIG. 1: Running coupling $1/g^2$ vs. a/L. The crosses are from simulations with $\beta_6 = 0$ (Ref. [4] and Table IV): top to bottom, $\beta = 5.8$, 5.4, 5.0, 4.8, 4.6, and 4.4. The circles are from simulations with $\beta_6 = 0.5$ (Table III): top to bottom, $\beta = 3.5$, 2.5, and 2.0. The straight lines are linear fits [Eq. (5)] to each set of points at given (β, β_6); the slope gives the beta function. The dotted line shows the expected slope from one-loop running.

III. BETA FUNCTION

The computation of the running coupling proceeds exactly as described in Ref. [4], with the same boundary conditions on the fermion and gauge fields. In brief, one imposes Dirichlet boundary conditions at the time slices $t = 0, L$, and measures the response of the quantum effective action. The coupling emerges from a measurement of the derivative of the action with respect to a parameter η in the boundary gauge field,

$$\frac{K}{g^2(L)} = \left\langle \frac{\partial S_G}{\partial \eta} - \mathrm{tr}\left(\frac{1}{D_F^\dagger} \frac{\partial (D_F^\dagger D_F)}{\partial \eta} \frac{1}{D_F} \right) \right\rangle \Bigg|_{\eta=0} . \tag{3}$$

The constant K can be calculated directly from the classical continuum action. Only g_0, Eq. (2), appears in the latter, which assures that $K = 12\pi$ regardless of β_6.

We presented in Ref. [4] the values of the running coupling g^2 for a number of values of (β, κ_c) with $\beta_6 = 0$. Our new results for $\beta_6 = 0.5$ are shown in Table III, with supplementary data on new volumes for $\beta_6 = 0$ shown in Table IV. Both sets are plotted in Fig. 1.[2]

[2] We have dropped from consideration the data given in [4] for $(\beta, \beta_6) = (4.3, 0)$ since these were taken in a metastable state beyond the first-order boundary.

TABLE III: Running coupling, Eq. (3), evaluated at the bare coupling (β, κ_c) with $\beta_6 = 0.5$ on lattices of size L. The omission of the result for $L = 16a$ at $\beta = 2.0$ is explained in the text.

β	$1/g^2$					
	$L = 6a$	$L = 8a$	$L = 10a$	$L = 12a$	$L = 14a$	$L = 16a$
3.5	0.2918(13)	0.2859(48)	0.2888(53)	0.2703(58)	–	–
2.5	0.1454(32)	0.1433(45)	0.1424(42)	0.1517(36)	0.1647(65)	0.1449(68)
2.0	0.0915(32)	0.1023(37)	0.0942(56)	0.1057(51)	–	*

TABLE IV: Running coupling for the strong-coupling cases with $\beta_6 = 0$. Data for $L = 10a, 14a$ are from the new simulations listed in Table II, while the other data are from Ref. [4]. Data for $\beta = 4.6$ were taken with $\kappa = \kappa_c = 0.13320$.

β	$1/g^2$					
	$L = 6a$	$L = 8a$	$L = 10a$	$L = 12a$	$L = 14a$	$L = 16a$
4.8	0.3151(50)	0.3002(28)	0.3013(61)	0.3008(45)	–	–
4.6	0.2692(27)	0.2615(41)	–	0.2525(50)	–	0.2289(56)
4.4	0.2191(24)	0.2103(34)	0.2021(66)	0.2080(50)	0.2235(105)	0.2119(53)

It is convenient to define the beta function $\tilde{\beta}(u)$ for $u \equiv 1/g^2$ as

$$\tilde{\beta}(u) \equiv \frac{d(1/g^2)}{d\log L} = 2\beta(g^2)/g^4 = 2u^2\beta(1/u) \qquad (4)$$

in terms of the conventional beta function $\beta(g^2)$. As discussed in Ref. [6], the slow running of the coupling suggests extracting the beta function at each (β, κ_c) from a linear fit of the inverse coupling

$$u(L) = c_0 + c_1 \log \frac{L}{8a} \ . \qquad (5)$$

With this parametrization, c_0 gives the inverse coupling $u(L = 8a)$, while c_1 is an estimate for the beta function $\tilde{\beta}$ at this coupling.

For a first look, we fit the data points for *all* L to extract the slopes at the given bare parameters, ignoring discretization errors that must be inherent in the smallest lattices. These fits are shown in Fig. 1. Values of the beta function $\tilde{\beta}(u)$ obtained from these fits are plotted as a function of $u(L = 8a)$ in Fig. 2. One can see that the results for $\beta_6 = 0$ and for $\beta_6 = 0.5$ are consistent with each other. Also shown are the one- and two-loop approximations from the expansion

$$\tilde{\beta}(u) = -\frac{2b_1}{16\pi^2} - \frac{2b_2}{(16\pi^2)^2}\frac{1}{u} + \cdots, \qquad (6)$$

where $b_1 = 13/3$ and $b_2 = -194/3$.

The assumption behind the linear fits is that $\tilde{\beta}$ is small so that $u(L/a)$ changes very slowly with the volume; this behavior is apparent in Fig. 1. Nonetheless, where there are four or more volumes to be fitted for a given coupling the χ^2 is not particularly good. Corrections to the approximate Eq. (5) come from discretization errors, as well as from the slight deviation from constancy of the continuum beta function over the range of volumes. We defer consideration of discretization errors to Sec. V. Variation of the continuum beta function gives rise to higher powers of $\log L$. Adding the next-to-leading term, at each bare coupling we fit

$$u(L) = c_0 + c_1 \log L/8a + c_2(\log L/8a)^2. \qquad (7)$$

From the definition of a beta function it follows that c_1 continues to provide an estimate for $\tilde{\beta}$ at $u = 1/g^2(L = 8a)$. The results of these fits are shown as empty symbols in Fig. 2. It is evident that there is only a small change compared to the linear fits of Eq. (5). In our analysis of discretization error, given below, we use only the single logarithm.

At the two strongest couplings the beta function plotted in Fig. 2 is positive, indicating the existence of an infrared fixed point. As we shall see, this conclusion does not survive consideration of the discretization error. It is possible that the beta function remains negative even at the strongest couplings studied. Hence, we cannot rule out a "walking" scenario wherein the beta function comes close to zero, but never actually turns positive.

Nevertheless, Figs. 1 and 2 demonstrate an important qualitative result, which will be unaltered by any analysis of lattice error: The coupling constant runs more slowly than one-loop perturbation theory over the entire range of bare parameters. This is in marked contrast to QCD, where the running coupling runs faster than the one-loop (or the two-loop) beta function as one enters strong coupling [23].

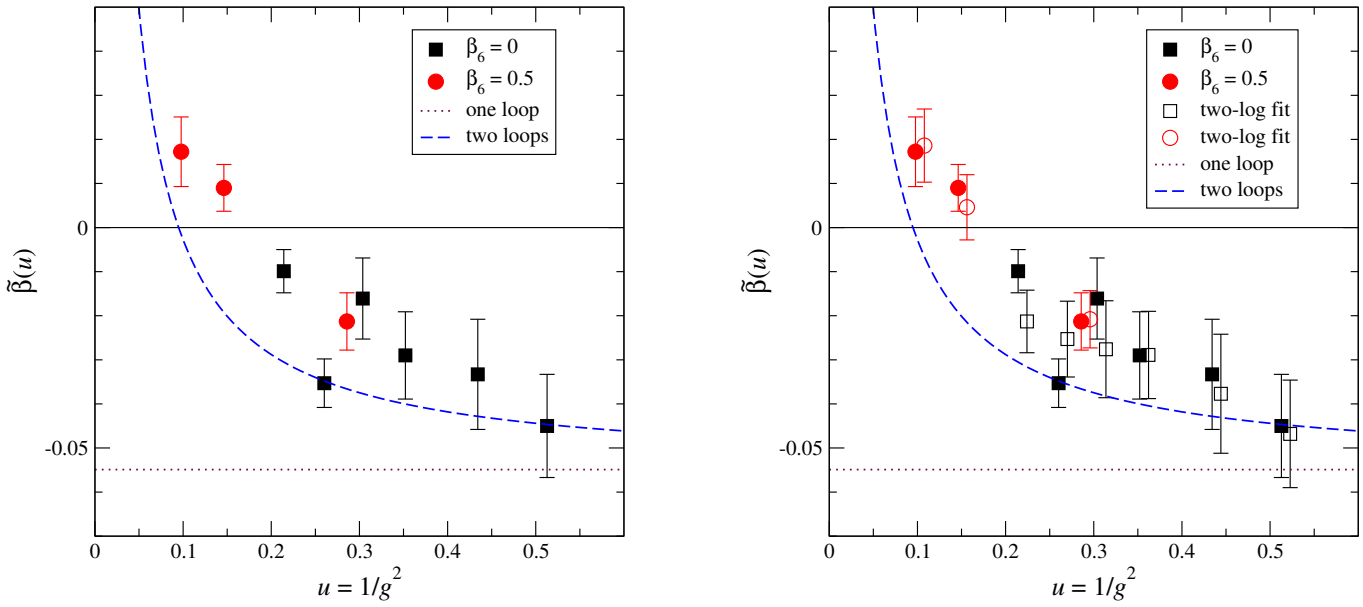

FIG. 2: Left: Beta function $\tilde{\beta}(u)$ plotted as a function of $u(L = 8a)$. The squares are from the $\beta_6 = 0$ data while the circles are from $\beta_6 = 0.5$. Results are extracted from the linear fits (5), as shown in Fig. 1. Plotted curves are the one-loop (dotted line) and two-loop (dashed line) beta functions. Right: Filled symbols as on left; empty symbols derive from fits to Eq. (7), in which a $\log^2$ term has been added. The empty symbols have been slightly displaced to the right. No correction has been made for discretization errors.

IV. MASS ANOMALOUS DIMENSION

We derive the mass anomalous dimension from the scaling with L of the pseudoscalar renormalization factor Z_P. The latter is calculated by taking the ratio

$$Z_P = \frac{c\sqrt{f_1}}{f_P(L/2)}. \tag{8}$$

f_P is the propagator from a wall source at the $t = 0$ boundary to a point pseudoscalar operator at time $L/2$. The normalization of the wall source is removed by the f_1 factor, which is a boundary-to-boundary correlator. The constant c, which is an arbitrary normalization, is $1/\sqrt{2}$ in our convention.

We present in Tables V and VI the results of calculating Z_P in our runs with $\beta_6 = 0.5$ and with $\beta_6 = 0$; we plot them in Fig. 3.

The slow running suggests [6] that we may extract γ_m by applying the approximate scaling formula

$$Z_P(L) = Z_P(L_0)\left(\frac{L_0}{L}\right)^{\gamma}, \tag{9}$$

that is, from the slopes of the lines drawn in Fig. 3. These linear fits are analogous to Eq. (5):

$$\log Z_P(L) = c_0 + c_1 \log\frac{L}{8a}. \tag{10}$$

Again, we begin by fitting to all volumes at a given bare coupling simultaneously, leaving for later the discretization errors due to the smallest lattices. The individual

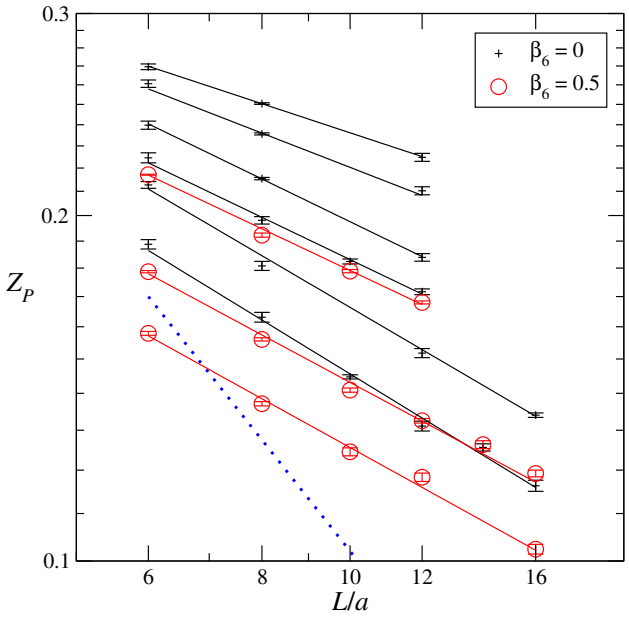

FIG. 3: The pseudoscalar renormalization constant Z_P vs. L/a. The crosses are from simulations with $\beta_6 = 0$, $\beta = 5.8$ to 4.4. The circles are from simulations with $\beta_6 = 0.5$ (Table V): top to bottom, $\beta = 3.5$, 2.5, and 2.0. The straight lines are linear fits to each set of points at given (β, β_6); the slope gives $-\gamma_m$. The hypothetical dotted line corresponds to $\gamma_m = 1$.

TABLE V: Pseudoscalar renormalization factor Z_P evaluated at the couplings (β, κ_c), with $\beta_6 = 0.5$, for lattice sizes L.

β	Z_P					
	$L = 6a$	$L = 8a$	$L = 10a$	$L = 12a$	$L = 14a$	$L = 16a$
3.5	0.2171(2)	0.1923(8)	0.1789(6)	0.1680(5)	–	–
2.5	0.1787(4)	0.1560(5)	0.1409(6)	0.1325(6)	0.1263(10)	0.1192(8)
2.0	0.1579(6)	0.1371(6)	0.1245(10)	0.1183(10)	–	0.1024(10)

TABLE VI: Pseudoscalar renormalization factor Z_P for the strong-coupling cases with $\beta_6 = 0$. Data for $L = 10a, 14a$ are from the new simulations listed in Table II, while the other data are from Ref. [4].

β	Z_P					
	$L = 6a$	$L = 8a$	$L = 10a$	$L = 12a$	$L = 14a$	$L = 16a$
4.8	0.2246(23)	0.1981(15)	0.1824(9)	0.1716(10)	–	–
4.6	0.2127(14)	0.1808(16)	–	0.1518(14)	–	0.1340(6)
4.4	0.1888(18)	0.1631(16)	0.1447(6)	0.1311(13)	0.1256(9)	0.1163(13)

fits are shown as straight lines in Fig. 3. The outstanding feature of Fig. 3 is that in no case does the slope of any data set approach -1, meaning that γ_m (Fig. 4) never reaches unity. This qualitative observation survives all further analysis.

Allowing for running of the coupling, we have also considered a fit function analogous to Eq. (7),

$$\log Z_P(L) = c_0 + c_1 \log L/8a + c_2 (\log L/8a)^2. \qquad (11)$$

For both fits the mass anomalous dimension at $g^2(L = 8a)$ is given by $-c_1$. We show the results of both fit types in Fig. 4, plotted against the running coupling $g^2(L = 8a)$. It is apparent that the result for $\gamma_m(g^2)$ changes little when the fit is broadened, or in other words, that scaling violations due to the nonzero beta function are small.

A comparison of results for the two lattice actions shows that there is some disagreement. The two strongest-coupling points obtained with $\beta_6 = 0$ lie well above the line connecting the $\beta_6 = 0.5$ points. As we shall see, analysis of discretization errors reduces this discrepancy. Moreover, the rough bound $\gamma_m \lesssim 0.5$ will be strengthened by extrapolation to the continuum limit.

V. ESTIMATING DISCRETIZATION ERROR

Before showing our extrapolations to the continuum/infinite volume limit, let us make some general comments.

Lattice studies of quantum chromodynamics approach the continuum limit in the weak-coupling regime. QCD possesses a physical scale Λ. A systematic approach to discretization error gives an expansion of physical quantities in powers of Λa, with which one may extrapolate to the $a \to 0$ limit. Perturbation theory gives a guide to the coefficients in the expansion. The $L \to \infty$ limit is taken separately; it is governed by the mass gap M of the theory and the corrections are functions of ML.

The theory considered here differs from lattice QCD in several essential features. In the first place, the coupling runs much more slowly than in QCD. After all, the theory was selected for study because this is true in the two-loop beta function; our numerical results bear this out nonperturbatively. In the second place, we seek the putative infrared fixed point in strong coupling. Along with a strong SF coupling at the volume scale L, then, we have slow running to a still-strong coupling at the lattice scale a. There is a perturbative scale Λ_1 that emerges from one-loop running, but it never comes into play. Much as in truly conformal theories, discretization errors are functions of a/L—they are indistinguishable from finite-volume corrections. It is clear from this that any perturbative estimate of discretization error is pointless.

Nonetheless, we offer a discussion of the fermion contribution to the one-loop SF coupling in the appendix. We point out that, even were we to work at couplings where one-loop perturbation theory is valid, for our lattices the $O(a^2/L^2)$ corrections are so large that they cannot be disentangled from $O(a/L)$. This means that any fit function used to extrapolate to $a/L = 0$ constitutes a model rather than an expansion about the limit.

Since our main result is the upper bound on the anomalous dimension γ_m, we begin with the analysis of discretization error in this quantity. We focus on the strong-coupling data displayed in Tables V and VI. The $\beta_6 = 0.5$ data show the dramatic departure of $\gamma(g^2)$ from the one-loop line (see Fig. 4). Comparison to the $\beta_6 = 0$ shows an apparent discrepancy between the two actions that begs explanation. We present several extrapolations to $a/L = 0$, which result in a systematic shift downwards of the results. At the same time, the results from the two

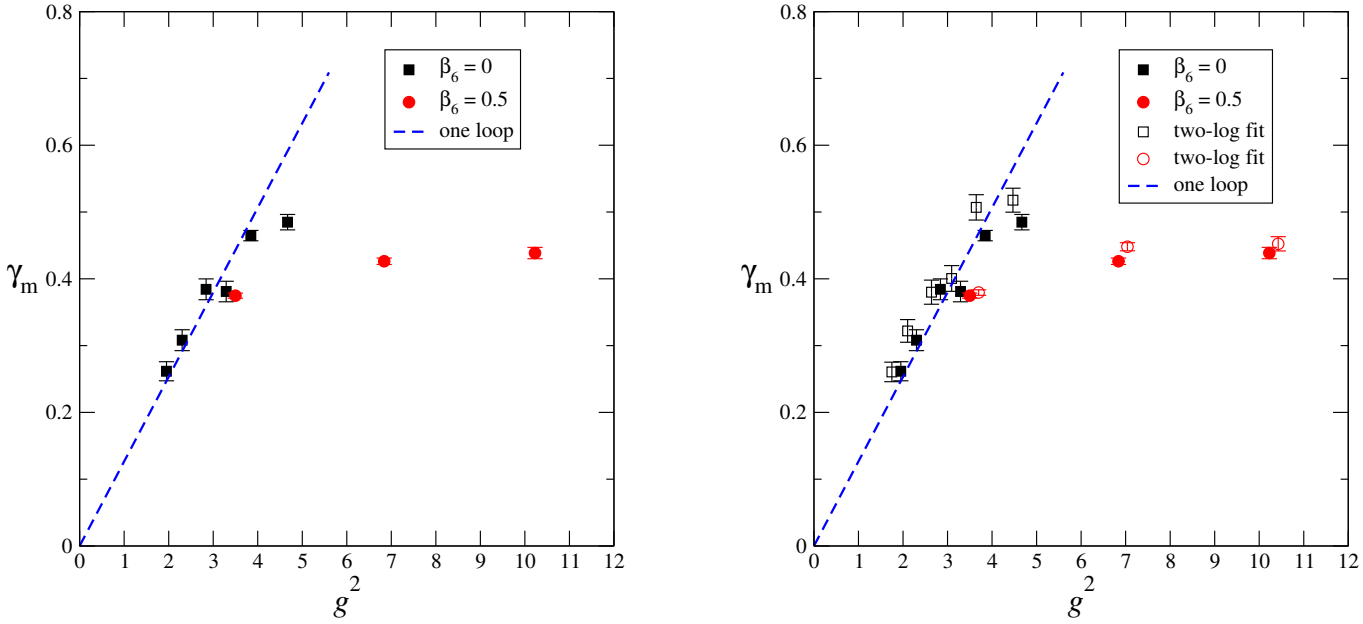

FIG. 4: Left: Mass anomalous dimension $\gamma(g^2)$ plotted against $g^2(L = 8a)$. The squares are from the $\beta_6 = 0$ data while the circles are from $\beta_6 = 0.5$. Results are from the linear fits shown in Fig. 3. The line is the one-loop result. Right: Filled symbols as on left; empty symbols derive from fits to Eq. (11), in which a $\log^2$ term has been added. The empty symbols have been slightly displaced horizontally. No correction has been made for discretization errors.

actions are brought closer to agreement, both through the propagation of statistical error in the extrapolation and through uncertainty surrounding the method of extrapolation to $a/L = 0$.

Similar analyses of the beta function are inconclusive. The dependence of the running coupling g^2 on lattice size L is irregular and not amenable to smooth extrapolation to the continuum. In the end, we have to let our lattice results stand as they are.

A. Anomalous dimension

The general behavior we expect for $Z_P(L)$ is

$$Z_P(L) = A \exp\left[-\int^1 \frac{dt}{t}\,\gamma_m\left(g^2(tL)\right)\right] + P_1\frac{a}{L} + P_2\left(\frac{a}{L}\right)^2 + \cdots. \tag{12}$$

For a slowly-running coupling, the first term simplifies to $A\,(L/a)^{-\gamma_m(g^2)}$. The original procedure [36] is to extract the step scaling function $\sigma_P(g^2, s)$ from the ratio of Z_P measured on two lattices,

$$\sigma_P(v, s) = \left.\frac{Z_P(sL)}{Z_P(L)}\right|_{g^2(L)=v}. \tag{13}$$

For slow running, this is just

$$\sigma_P(g^2, s) = s^{-\gamma_m(g^2)}. \tag{14}$$

The traditional analysis[3] continues by computing $\sigma_P(g^2, s)$ at fixed s for several values of L and extrapolating L to infinity. Let us begin our analysis by doing variations on the traditional fit.

1. *Extrapolation of the step scaling function*

At[4] $\beta = 4.4$, 4.6, and 2.0, 2.5, we can do the most traditional fit of all: fix the ratio $s = 2$ and compare σ_P for the pair $L = (6a, 12a)$ with $L = (8a, 16a)$. The results for

$$\gamma_m(L) = \frac{\log \sigma_P}{\log 2} \tag{15}$$

are plotted in Fig. 5 against L of the smaller lattice.

In all four cases,there is a discernible L dependence in the data. Now we face the problem of how to extrapolate in L. As noted above, we are away from any perturbative limit, and so theory cannot guide us. Choosing models, we perform extrapolations linearly in L,

$$\gamma_m(L) = \gamma_m + C\frac{a}{L}, \tag{16}$$

[3] The truly traditional analysis keeps g^2 fixed by varying the bare couplings as L is changed. As we do throughout this paper, we take advantage of the slow running to do our analyses at fixed (β, β_6). The variation of g^2 is negligible.

[4] We sometimes refer to the data sets by their β values. The tables show that there is no confusion if we omit mention of β_6.

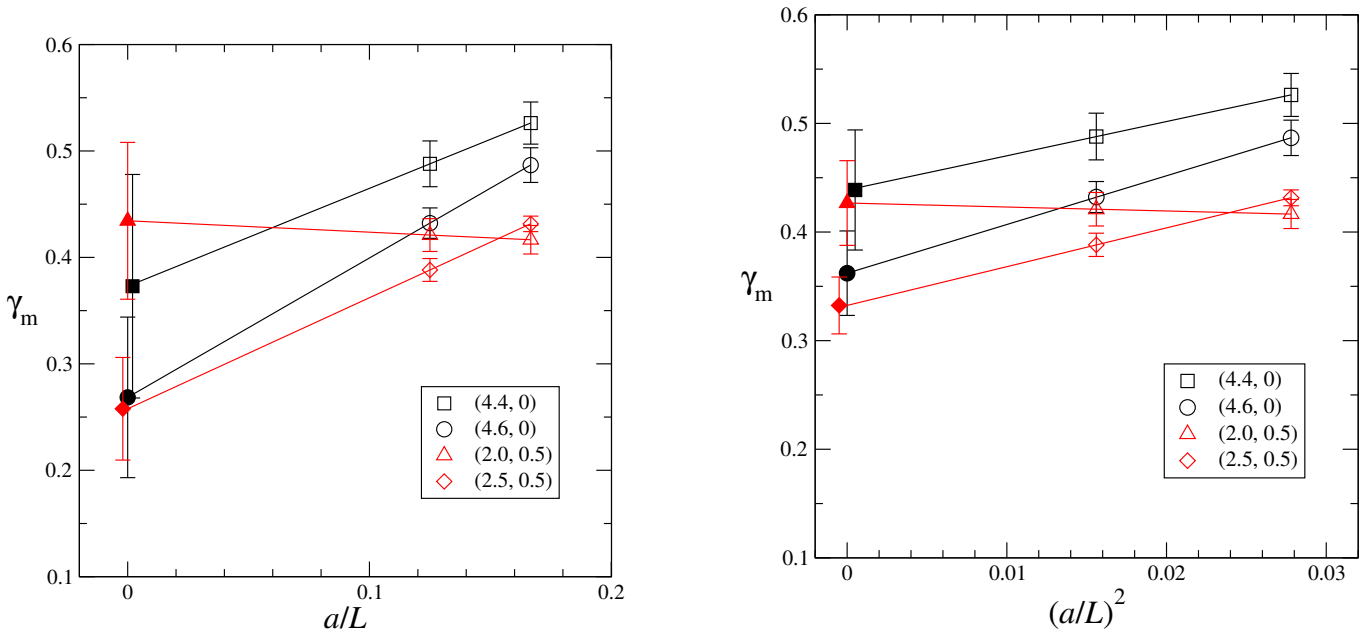

FIG. 5: γ_m from "traditional" fits to pairs of lattices $(L, 2L) = (6a, 12a)$ and $(8a, 16a)$, plotted versus a/L (left) and versus $(a/L)^2$ (right). The extrapolated values are shown near the origin. Couplings (β, β_6) are as shown.

or quadratically,

$$\gamma_m(L) = \gamma_m + C\left(\frac{a}{L}\right)^2. \tag{17}$$

The fits, with their extrapolations to $a/L = 0$, are shown in the figure and tabulated in Table VII. Because our fits are of two points to two parameters, there is no goodness-of-fit criterion to invoke: The data cannot express a preference between the models.

The extrapolations to $a/L = 0$ show a (mostly) downward trend compared to any individual σ_P. The resulting error bars are of course larger but γ_m never exceeds 0.5 for any of the couplings examined. We defer further discussion of this sort until we reach the results of our all-volume analysis below.

In principle, we can judge the quality of the fits if we add data points, that is, more lattice volumes. To this end we have run simulations for lattices of size $L = 10a$ and $14a$ at two of the couplings, $\beta = 2.5$ and 4.4. This gives us three independent pairs of volumes from which to calculate a step scaling ratio. We use the pairs $L/a =$ (6, 12), (8,14), and (10,16) to calculate $\sigma_P(g^2, s)$ for $s =$ 2, 7/4, and 8/5, respectively, and estimate

$$\gamma_m(L) = \frac{\log \sigma_P(g^2, s)}{\log s} \tag{18}$$

as a function of the smaller L of each pair. Fig. 6 shows the result, together with the extrapolations to infinite L—now two-parameter fits to three points, which are also tabulated in Table VII. The quality of the fits is good in all cases, so (unfortunately) the data do not express a choice between $1/L$ and $1/L^2$ corrections.

β	L pairs	γ_m	
		linear fit	quadratic fit
4.4	(6,12),(8,16)	0.37(10)	0.44(5)
4.6	(6,12),(8,16)	0.27(7)	0.36(4)
2.0	(6,12),(8,16)	0.43(7)	0.43(4)
2.5	(6,12),(8,16)	0.26(5)	0.33(3)
4.4	(6,12),(8,14),(10,16)	0.35(6)	0.42(4)
2.5	(6,12),(8,14),(10,16)	0.23(4)	0.31(3)

TABLE VII: "Traditional" extrapolations of γ_m from the pairwise step scaling function σ_P.

2. *All-volume extrapolations*

Now we present a procedure for using data from all volumes simultaneously to arrive at the extrapolated γ_m at each value of the bare coupling. The most straightforward approach would be to take the measurements of Z_P and fit them to

$$\log Z_P(L) = A + \gamma_m \log(a/L) + c\frac{a}{L} \tag{19}$$

or to

$$\log Z_P(L) = A + \gamma_m \log(a/L) + c\left(\frac{a}{L}\right)^2. \tag{20}$$

We find, however, that our data do not distinguish well among the basis functions in these fits and hence the determinations of the parameters are unstable. We therefore adopt an alternative approach to estimation of the discretization error.

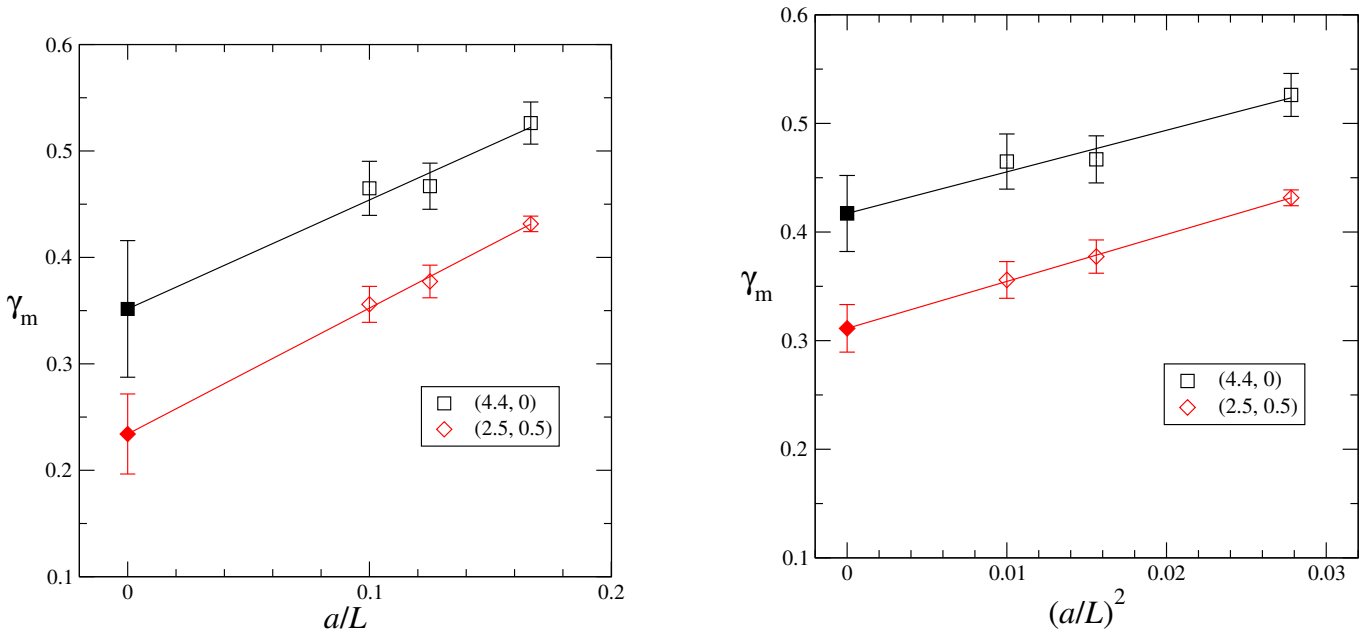

FIG. 6: γ_m from fits to three pairs of lattices $(L, L') = (6a, 12a)$, $(8a, 14a)$, and $(10a, 16a)$, plotted versus a/L (left) and versus $(a/L)^2$ (right). The extrapolated values are shown at the origin.

For each bare coupling β we have measured Z_P on a set of volumes $L_1 < L_2 < \ldots < L_N$. The comparison in Fig. 4 shows that the running of the coupling is slow enough to be neglected over the range $L_1 \le L \le L_N$. The only obstruction to extracting γ from a fit to Eq. (10) is then discretization error. Since this error is most pronounced at the smallest L's, we can improve our estimate of the true γ by successively dropping the smaller volumes. This observation is the basis for the following continuum extrapolation.

Let $c_0^{(n)}, c_1^{(n)}$ be the parameters of the linear fit (10) where only the largest volumes $L_n, L_{n+1}, \ldots, L_N$ are retained. The slope $c_1^{(n)}$ is an estimate for $-\gamma$ which we take to be a function of a/L_n. For example, if $\{L_1, \ldots, L_4\} = \{6a, 8a, 10a, 12a\}$, a fit using all volumes gives an estimate $c_1^{(1)}$ of $-\gamma$ for $a/L = 1/6$; dropping the smallest volume gives the next estimate $c_1^{(2)}$ for $a/L = 1/8$; and dropping the two smallest volumes gives the estimate $c_1^{(3)}$ for $a/L = 1/10$. Finally we extrapolate these estimates to the continuum limit, $a/L \to 0$, by fitting to either Eq. (16) or Eq. (17).

When performing the continuum extrapolation, we must take into account that the results $c_1^{(n)}$ of the successive fits are correlated. For the example above, with a maximum of two volumes dropped, it can be shown that the covariance matrix $\mathcal{C}_{mn} = \mathrm{cov}\left(c_1^{(n)}, c_1^{(m)}\right)$ is

$$\mathcal{C} = \begin{pmatrix} \Delta^{(1)} & \Delta^{(1)} & \Delta^{(1)} \\ \Delta^{(1)} & \Delta^{(2)} & \Delta^{(2)} \\ \Delta^{(1)} & \Delta^{(2)} & \Delta^{(3)} \end{pmatrix} , \qquad (21)$$

where $\Delta^{(n)} = \sigma^2\left(c_1^{(n)}\right)$ is the variance of each $c_1^{(n)}$.

We show in Fig. 7 the linear and quadratic continuum extrapolations for $\beta = 2.5$ and 4.4, where we can work from six volumes. In each case the fit has very low χ^2 as long as we exclude the final (leftmost) data point, which is based on $L/a = 14$ and 16 only. Since its error bar is large, omitting this point from the fit leaves the extrapolation unchanged. This is a feature of all the fits in the all-volume extrapolations.

To give an idea of the stability of our fit procedures, we compare them all (as available) in Fig. 8. We display the results of the all-volume extrapolations for all bare couplings in Table VIII, and we plot them in Fig. 9. Every point lies lower than the corresponding point in Fig. 4, which shows the result of the naive analysis. Correction for discretization error has pushed our bound on γ_m downward. In addition, the gap between the two actions ($\beta_6 = 0$ vs. 0.5) has narrowed, for two reasons. One is the larger error bars compared to Fig. 4; the other is the systematic uncertainty hovering over the choice between linear and quadratic continuum extrapolations.

B. Beta function

We would like to perform a similar analysis for the running coupling. Unfortunately, the data do not permit the extraction of extrapolated results carrying useful uncertainties. The reason why can quickly be seen from Fig. 10: The data at each individual bare coupling are irregular functions of L. This may mean that the error

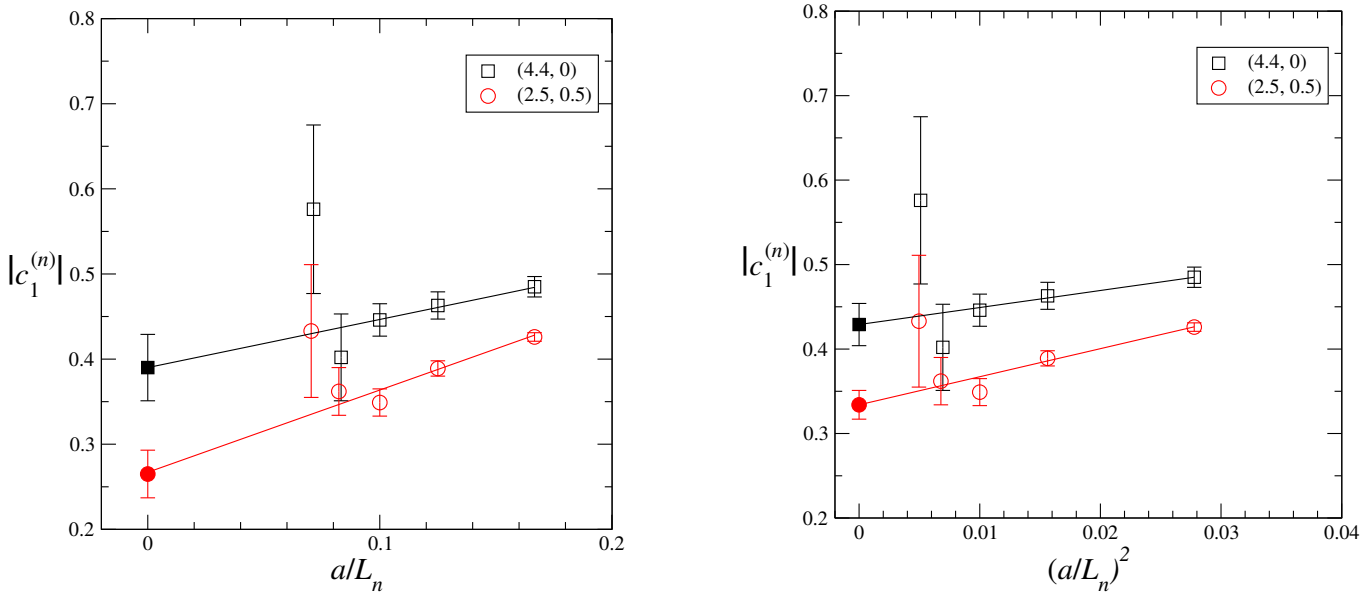

FIG. 7: Examples of linear and quadratic continuum extrapolations of the mass anomalous dimension $\gamma(g^2)$ derived from all-volume extrapolations. Values of (β, β_6) are as shown.

β	L values	γ_m	
		linear fit	quadratic fit
4.8	6,8,10,12	0.27(7)	0.32(4)
4.6	6,8,12,16	0.35(4)	0.40(3)
4.4	6,8,10,12,14,16	0.39(4)	0.43(3)
3.5	6,8,10,12	0.24(5)	0.29(3)
2.5	6,8,10,12,14,16	0.26(3)	0.33(2)
2.0	6,8,10,12,16	0.33(4)	0.37(3)

TABLE VIII: Continuum limit of γ_m from all-volume extrapolations.

bars for the individual data points are underestimated. The SF observable (3) generally has a very long autocorrelation time. For lattice sizes $L \geq 10a$, we determined an error bar by fitting four runs to a common constant, and collecting data until the χ^2 per degree of freedom from this fit fell below about two. This may not have been good enough. From a practical point of view, the pattern of our data makes analysis of the discretization errors quite difficult.

We shall treat only two data points: $\beta = 2.0$ and 2.5, with $\beta_6 = 0.5$. These are our strongest couplings, and as seen in Fig. 2 they hint at a positive beta function and hence an infrared fixed point.

At $\beta = 2.0$ we have four volumes: $L = 6a, 8a, 10a, 12a$. (We have discarded $L = 16a$ as discussed above.) For an almost traditional analysis we take them as two pairs, $(6a, 10a)$ and $(8a, 12a)$, and for each pair we calculate the discrete beta function (DBF),

$$B(u,s) = \frac{1}{g^2(sL)} - \frac{1}{g^2(L)}, \qquad u \equiv \frac{1}{g^2(L)} \ . \tag{22}$$

The scale factor s is 5/3 for the first pair and 3/2 for the second pair. The two DBFs can be combined if we rescale them according to

$$R(u,s) = \frac{B(u,s)}{\log s} \ . \tag{23}$$

This rescaled DBF approximates the usual beta function $\tilde{\beta}(1/g^2)$ when the running is slow [6]. We can plot it against the smaller L in each pair and extrapolate to $a/L = 0$ either linearly or quadratically, much as we did for γ_m above.

At $\beta = 2.5$ we have six volumes. Following our procedure for γ_m, we can first calculate the DBF for $s = 2$, using the pairs $(L, 2L) = (6a, 12a)$ and $(8a, 16a)$. Extrapolations to $a/L = 0$ then follow. Additionally, we calculate the rescaled DBF $R(u,s)$ for the three pairs $(L, L') = (6a, 12a)$, $(8a, 14a)$, and $(10a, 16a)$, and extrapolate it to a/L=0. Unfortunately, the irregularity of the data seen in Fig. 10 renders the three-pair fit useless: Trying to fit a straight line through the three points gives an enormous χ^2. The two-pair fits, of course, have no degrees of freedom and hence no χ^2.

At both couplings we can do all-volume extrapolations as for Z_P, *mutatis mutandis*. We fit to Eq. (5) to obtain coefficients $c_0^{(n)}, c_1^{(n)}$, where n indicates the smallest volume L_n retained in the fit. Finally we extrapolate to $a/L = 0$ either linearly or quadratically.

For $\beta = 2.0$ the all-volume extrapolations give reasonable χ^2 and improve on the pairwise extrapolations,

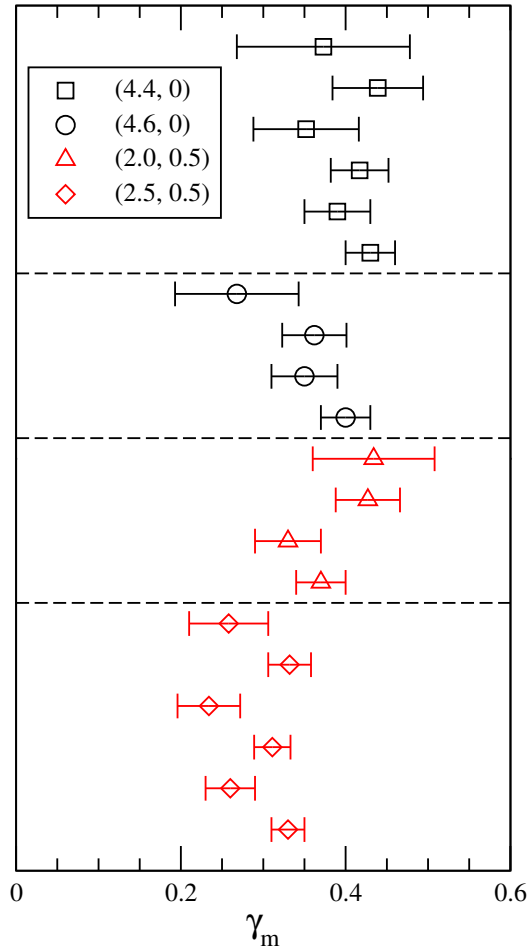

FIG. 8: Comparison of the results of all continuum extrapolations for the anomalous dimension at four bare couplings. For each coupling, we plot in sequence, top to bottom: two-pair extrapolations—linear and quadratic (Fig. 5); three-pair extrapolations (where available)—linear and quadratic (Fig. 6); all-volume extrapolations—linear and quadratic (Table VIII and Fig. 7).

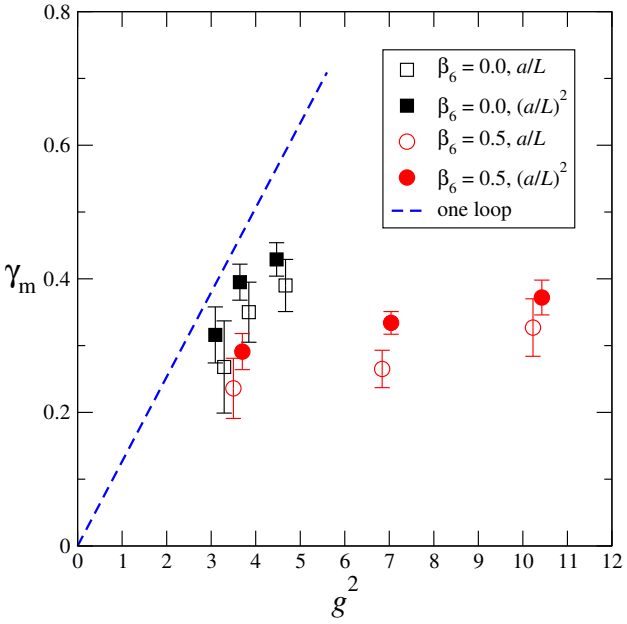

FIG. 9: Continuum limit of the mass anomalous dimension $\gamma(g^2)$ derived from all-volume extrapolations (see Table VIII, and compare Fig. 4). The squares are from the $\beta_6 = 0$ data while the circles are from $\beta_6 = 0.5$. Empty symbols assume discretization errors proportional to a/L while filled symbols assume $(a/L)^2$. The filled symbols have been slightly displaced horizontally.

as may be seen in Fig. 11. Nonetheless, the error bar for each extrapolation has grown by a factor of 4–6 compared to the raw fit shown in Figs. 1 and 2, which wipes out any sign of a zero crossing. For $\beta = 2.5$ the all-volume extrapolations give positive results but, again, the error bar has grown by a factor of 4–6 and the central values lie barely 1σ above zero. We therefore cannot confirm the existence of an infrared fixed point. It is quite possible that the beta function approaches zero as seen in Fig. 2 but then veers away, staying negative and leading to strong coupling at large distance. This would be exactly the behavior conjectured for walking technicolor.

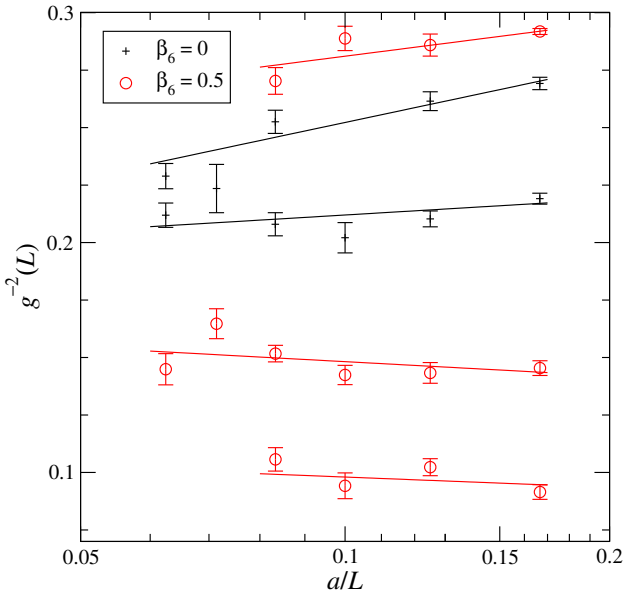

FIG. 10: A blown-up view of Fig. 1, showing the strong-coupling portion of our data sets for the running coupling $1/g^2$.

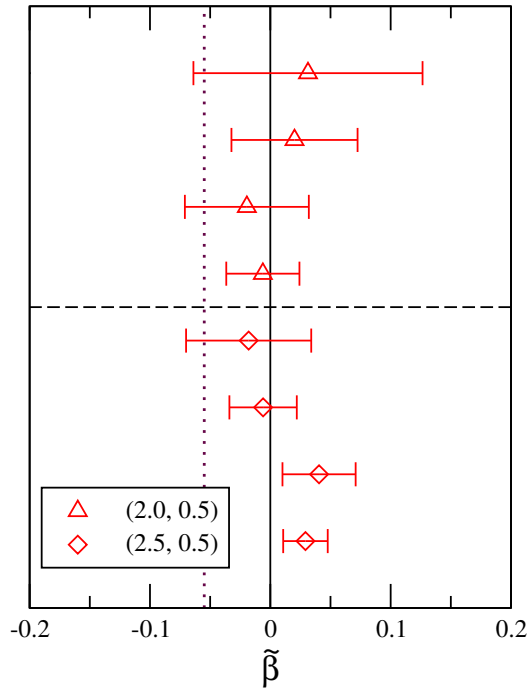

FIG. 11: Results of continuum extrapolations for the beta function at the two strongest couplings. For each (β, β_6) we plot in sequence, top to bottom, the two-pair extrapolations—linear and quadratic—and the all-volume extrapolations—linear and quadratic. The vertical dotted line is the one-loop value.

VI. DISCUSSION

In this paper we have continued our study of the SU(3) gauge theory with two flavors of sextet fermions. A new term in the lattice action allowed us to explore a much wider range of the renormalized coupling. The old and new actions give rise to consistent results for the beta function where they overlap. For the mass anomalous dimension there are some disagreements; we believe that the main source of the disagreement is the proximity of the first-order phase transitions—a lattice artifact—in the old action. The discrepancies are reduced when we extrapolate to the continuum limit.

We have developed a novel method to approach the continuum limit. It begins with the observation that, in a truly conformal theory, there is only a single expansion of lattice artifacts in powers of a/L. This is in sharp contrast with QCD, which generates its own scale dynamically, and therefore requires separate expansions for the discretization error and for finite-volume corrections. In the slowly running theory, deviations from exact conformality can in principle be treated systematically. In order to overcome difficulties in resolving fit functions in the range of a/L available to us, we developed a method of extrapolation based on successively dropping the smallest lattices. The differences between linear and quadratic extrapolations, as seen in Fig. 8, are an indication of our systematic error.

A. An infrared fixed point?

The question of the existence of an IRFP in this model has been addressed in the literature in several ways. A first hint comes from qualitative features of the phase diagram of the lattice theory [4, 5]. In QCD on a finite lattice, there is a confining phase for sufficiently strong coupling within which one may tune $\kappa \to \kappa_c$ in order to obtain a massless pion. Then one can increase the size of the lattice while tuning towards weak coupling on the $\kappa_c(\beta)$ curve, thus approaching the continuum limit within the confining phase. In the sextet theory, on the other hand, the confining phase is bounded by a first-order phase transition that does not permit definition of κ_c. It is not at all clear that a continuum limit in the confined phase would yield a theory with finite masses, let alone a chiral, massless limit. The only alternative might be to begin in the weak-coupling, non-confining phase, where one could take a non-confining continuum limit.

This feature of the phase diagram was first seen in QCD with a large number of (color-triplet) flavors by Iwasaki et al. [43, 44], and explored more recently in Ref. [45]. This may be a sign of entry into the conformal window in these theories. Turning to staggered fermions, the authors of Refs. [46, 47] have recently noted the absence of spontaneous breaking of chiral symmetry in strong-coupling (triplet) QCD when the number of flavors is large.

Even if one ignores the issue of a light pion, one can ask whether any kind of continuum limit can be taken in the confining phase. On a finite lattice, the first-order phase boundary at strong coupling connects to the boundary between strong-coupling and weak-coupling phases that may be interpreted as the finite-temperature phase transition. In a confining theory, this transition must move towards weak coupling as the lattice is enlarged, in such a way as to give a finite transition temperature in the continuum limit. In the theory with thin-link Wilson fermions, we found [2] that this motion stalls near the weak-coupling κ_c curve, as if the finite-temperature transition is avoiding the basin of attraction of an IRFP. More detailed study of this question in the fat-link theory [4] revealed a slow motion of the transition with lattice size; one would need to study larger lattices to see whether this motion eventually gives correct scaling in the continuum limit. In fact, because the perturbative running of the coupling is so slow [48], it will take enormous lattices to settle the matter. Kogut and Sinclair [49–52] have been studying the same question with staggered fermions; the results are, so far, similarly inconclusive.

Fodor *et al.* [53–57] have studied the staggered-fermion theory with extensive simulations on large volumes. On each lattice, they use quark masses that are large enough

that the volumes are effectively infinite. They then test alternative scaling hypotheses for the mass spectrum, the chiral condensate, f_π, and the string tension as a function of the quark mass. Their analysis favors confinement over conformal physics, meaning a beta function without an IRFP, which might behave as a walking theory.

As we have seen, our Schrödinger-functional results are not precise enough to nail down a fixed point. Statistical fluctuations preclude unambiguous extrapolation to the continuum limit. All we can say is that the beta function is smaller than the one-loop value, so that the theory runs slowly.

B. The mass anomalous dimension

As we have seen, γ_m first follows the one-loop curve and then at stronger couplings it levels off. This is in line with what we found in the SU(2) and SU(4) theories [6, 8]. The fits of Sec. IV, which do not take lattice error into account, give a bound

$$\gamma_m \lesssim 0.45\,. \tag{24}$$

At weak couplings we did not carry out a continuum extrapolation. At our strongest couplings, our analysis of discretization error (Sec. V) leads to larger error bars than our first analysis, but also to a general movement downwards so that our final result is the same bound (24).

The issue of scheme-dependence always arises at this point. The value of γ_m at a fixed point, if there is one, is scheme-independent. We can say more than this, however. A bound like Eq. (24) is evidently invariant under any redefinition $g \to g'(g)$, that is, it is entirely scheme-independent. A change of scheme will change the functional dependence of γ on the renormalized coupling, but if γ is bounded (and even flat) over a wide range of bare couplings then it will stay so.

A successful model of walking (extended) technicolor must have a slowly-varying coupling, but no infrared fixed point; it must also have a large mass anomalous dimension, $\gamma_m \simeq 1$. While our results do not rule out walking in the sextet theory, the smallness of γ_m makes this theory unsuitable for walking technicolor.

Acknowledgments

We thank Ohad Raviv for assistance in the preparation of the appendix, and Sara Beck for a valuable discussion. B. S. and Y. S. thank the University of Colorado for hospitality. This work was supported in part by the Israel Science Foundation under grant no. 423/09 and by the U. S. Department of Energy.

The computations for this research were made possible in part by the U. S. National Science Foundation through TeraGrid resources provided by (1) the University of Texas and (2) the National Institute for Computational Sciences (NICS) at the University of Tennessee, under grant number TG-PHY090023. Additional computations were done on facilities of the USQCD Collaboration at Fermilab, which are funded by the Office of Science of the U. S. Department of Energy. Our computer code is based on the publicly available package of the MILC collaboration [58]. The code for hypercubic smearing was adapted from a program written by A. Hasenfratz, R. Hoffmann and S. Schaefer [59].

Appendix: One loop analysis

In the one-loop approximation the SF coupling, defined in Eq. (3), takes the form

$$\frac{1}{g^2(L)} = \frac{1}{g_0^2} + \Sigma_G(L) + 2\Sigma_F(L)\,. \tag{A.1}$$

Here g_0 is the bare coupling from Eq. (2), and the one-loop contributions are Σ_G from the gauge and ghost fields[5] and Σ_F from each flavor of the sextet fermions. Following the definitions[6] and methodology of Ref. [21], two groups [60–63] have recently calculated the fermion piece Σ_F for a number of gauge groups and representations and for a variety of boundary conditions and background fields (as imposed in the SF method). On general grounds, one can expand

$$\begin{aligned}\Sigma_F(L) \;=\; & r_0 + s_0\log(L/a) + r_1\frac{a}{L} + s_1\frac{a}{L}\log(L/a) \\ & + r_2\frac{a^2}{L^2} + s_2\log(L/a)\frac{a^2}{L^2} + \cdots\,.\end{aligned} \tag{A.2}$$

The continuum limit consists of the first two terms on the right-hand side. The coefficient s_0 of the logarithmic term is the universal contribution of a fermion field to the one-loop beta function. The constant r_0 depends on the choice of the background field, *i.e.*, it introduces scheme dependence.

All other terms on the right-hand side of Eq. (A.2) constitute the discretization error. In the presence of a clover term with $c_{SW} = 1$ we have $s_1 = 0$. The remaining terms do not vanish in general. The linear discretization error (r_1 term) can be cancelled by adding a boundary counterterm for the gauge field. As for the quadratic discretization error (the r_2 term), one can suppress it by a judicious choice of the background field [60–62]. The outcome of adopting both measures is an improved one-loop behavior, where $s_1 = r_1 = r_2 = 0$.

The above strategy is natural for QCD, where the bare coupling is such that physics at the cutoff scale is typically well inside the perturbative regime. Here we are

[5] $\Sigma_G(L)$ has not been calculated for nHYP links.
[6] Our $\Sigma_F(L)$ is called $p_{1,1}$ in Ref. [21].

faced with a drastically different situation. Because of the slow running, in order to reach the interesting strong values of the renormalized coupling, the bare coupling must already be strong. As a result, we can no longer rely on perturbation theory at the quantitative level. Suffice it to mention that, in the vicinity of a two-loop fixed point, the two-loop contributions must be as important as the one-loop! Besides, the main thrust of the present paper is the calculation of the mass anomalous dimension for sextet fermions, for which no perturbative study of discretization errors has been carried out.

The conclusion, obviously, is not that discretization errors are to be ignored; as in any lattice simulation, a continuum extrapolation is mandatory. The point is that the continuum extrapolation must be done non-perturbatively. This is what we have attempted, with mixed success, in Sec. V.

We now proceed to a discussion of Σ_F for sextet fermions, in order to get some idea of the magnitude of this piece of the discretization error in the weak-coupling regime. We have computed Σ_F by following closely Appendix A of Ref. [21]. Inputs to the calculation are the fermion twist phase, set to $\theta = \pi/5$, and the classical background field, which, in turn, is determined by the SF boundary data. (nHYP smearing leaves the classical background field unchanged.) The spatial links on each time boundary are specified by three abelian phases $\phi_i = \phi_i(\eta)$, $i = 1, 2, 3$, which satisfy the constraint $\phi_1 + \phi_2 + \phi_3 = 0$. The corresponding six phases of the sextet representation are given by $\phi_{ij} = \phi_i + \phi_j$, with $1 \le i \le j \le 3$. Σ_F is written as a sum over the lattice 3-momentum $\mathbf{p}$. For each $\mathbf{p}$, the fermions' contribution can be represented as $\partial/\partial\eta \,\mathrm{tr}\, \log M\Big|_{\eta=0}$, where M is a two-by-two matrix that depends on $\mathbf{p}$ and on the boundary conditions [21].

We plot Σ_F as a function of L in Fig. 12. For comparison, we also show the continuum result $\widetilde{\Sigma}_F = r_0 + 5/(12\pi^2) \log L$, where the scheme-dependent constant r_0 has been extracted from a fit of Σ_F to the six terms shown in Eq. (A.2). In this fit, the coefficient s_0 is fixed at the continuum value and s_1 is fixed to zero (see above). The other coefficients are listed in Table IX.

In order to get an idea of the magnitude of discretization errors in the beta function, we plot Σ_F against $\log(a/L)$ in the second panel of Fig. 12; here we limit the range of L to $6a \le L \le 16a$ to match our numerical simulations. This plot is analogous to Fig. 1 (but note that here we display only the contribution of a single sextet fermion). The continuum result now shows up as a straight line, whereas the lattice result exhibits deviations from linearity. It can be seen that much of the discrepancy between the continuum and lattice results can be accounted for by an additive constant. As noted above, a constant shift r_0 does not represent a discretization error, but, rather, scheme dependence. The discretization error in the beta function will appear as a difference in the slopes of the two lines. Using the method of least squares to estimate the average slope of the lattice data we find the value 0.0446, which amounts to a 5% deviation from the correct continuum value $5/(12\pi^2) \simeq 0.0422$. Multiplying by two for the number of flavors, we conclude that the fermions' contribution to the discretization error in the beta function is in absolute terms roughly 0.005. A glance at Fig. 2 shows that this is a less than half the statistical error plotted for the weak-coupling data points.

TABLE IX: Free coefficients in the fit (A.2).

r_0	0.1569
r_1	−0.1914
r_2	0.4169
s_2	0.0086

The smallness of the deviation in the slope is connected to the coefficients r_1 and r_2 of the linear and quadratic lattice corrections. The two coefficients turn out to have opposite sign and magnitudes that cause their contributions to the slope to cancel. Thus one cannot really justify an expansion in powers of a/L in extrapolating to the continuum limit from our data. As we have stressed above, any given extrapolation is a model.

[1] Y. Shamir, B. Svetitsky and T. DeGrand, "Zero of the discrete beta function in SU(3) lattice gauge theory with color sextet fermions," Phys. Rev. D **78**, 031502 (2008) [arXiv:0803.1707 [hep-lat]].

[2] T. DeGrand, Y. Shamir and B. Svetitsky, "Phase structure of SU(3) gauge theory with two flavors of symmetric-representation fermions," Phys. Rev. D **79**, 034501 (2009) [arXiv:0812.1427 [hep-lat]].

[3] T. DeGrand, "Finite-size scaling tests for SU(3) lattice gauge theory with color sextet fermions," Phys. Rev. D **80**, 114507 (2009) [arXiv:0910.3072 [hep-lat]].

[4] T. DeGrand, Y. Shamir, B. Svetitsky, "Running coupling and mass anomalous dimension of SU(3) gauge theory with two flavors of symmetric-representation fermions," Phys. Rev. **D82**, 054503 (2010). [arXiv:1006.0707 [hep-lat]].

[5] B. Svetitsky, Y. Shamir and T. DeGrand, "Sextet QCD: slow running and the mass anomalous dimension," PoS LATTICE **2010**, 072 (2010) [arXiv:1010.3396 [hep-lat]].

[6] T. DeGrand, Y. Shamir, B. Svetitsky, "Infrared fixed point in SU(2) gauge theory with adjoint fermions," Phys. Rev. **D83**, 074507 (2011). [arXiv:1102.2843 [hep-lat]].

[7] T. DeGrand, Y. Shamir, B. Svetitsky, "Gauge theories with fermions in the two-index symmetric representation," [arXiv:1110.6845 [hep-lat]].

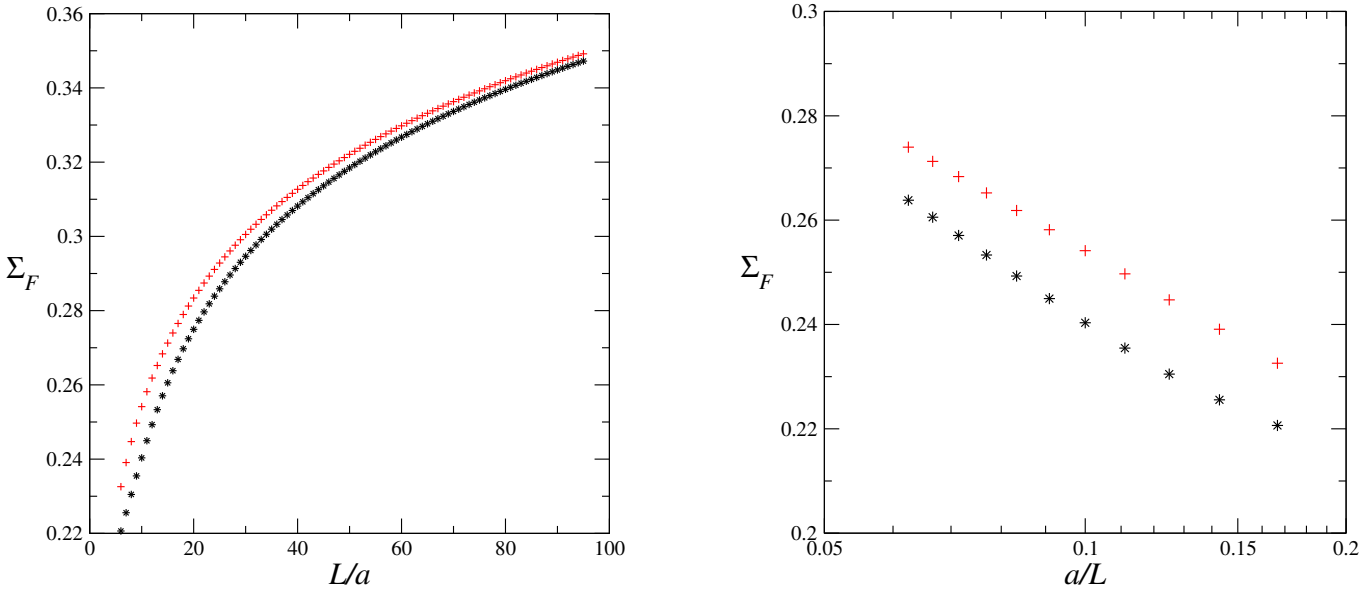

FIG. 12: The sextet fermions' contribution to the one-loop SF coupling as a function of lattice size. The exact result (stars) is compared to the continuum formula (crosses) wherein the arbitrary constant r_0 comes from a fit as discussed in the text. The second plot shows only $6a \leq L \leq 16a$, for comparison with Fig. 1.

[8] T. DeGrand, Y. Shamir and B. Svetitsky, "SU(4) lattice gauge theory with decuplet fermions: Schrödinger functional analysis," arXiv:1202.2675 [hep-lat].

[9] F. Sannino and K. Tuominen, "Orientifold theory dynamics and symmetry breaking," Phys. Rev. D **71**, 051901 (2005) [arXiv:hep-ph/0405209].

[10] D. K. Hong, S. D. H. Hsu and F. Sannino, "Composite Higgs from higher representations," Phys. Lett. B **597**, 89 (2004) [arXiv:hep-ph/0406200].

[11] D. D. Dietrich, F. Sannino and K. Tuominen, "Light composite Higgs from higher representations versus electroweak precision measurements: Predictions for LHC," Phys. Rev. D **72**, 055001 (2005) [arXiv:hep-ph/0505059].

[12] C. T. Hill and E. H. Simmons, "Strong dynamics and electroweak symmetry breaking," Phys. Rept. **381**, 235 (2003) [Erratum-ibid. **390**, 553 (2004)] [arXiv:hep-ph/0203079];

[13] B. Holdom, "Raising The Sideways Scale," Phys. Rev. D **24**, 1441 (1981).

[14] K. Yamawaki, M. Bando and K. i. Matumoto, "Scale Invariant Technicolor Model And A Technidilaton," Phys. Rev. Lett. **56**, 1335 (1986).

[15] T. Appelquist, J. Terning and L. C. R. Wijewardhana, "Postmodern technicolor," Phys. Rev. Lett. **79**, 2767 (1997) [arXiv:hep-ph/9706238].

[16] R. S. Chivukula and E. H. Simmons, "Condensate enhancement and D-meson mixing in technicolor theories," Phys. Rev. D **82**, 033014 (2010) [arXiv:1005.5727 [hep-lat]].

[17] D. B. Kaplan, J. -W. Lee, D. T. Son and M. A. Stephanov, "Conformality Lost," Phys. Rev. D **80**, 125005 (2009) [arXiv:0905.4752 [hep-th]].

[18] M. Lüscher, R. Narayanan, P. Weisz and U. Wolff, "The Schrodinger functional: A Renormalizable probe for non-Abelian gauge theories," Nucl. Phys. B **384**, 168 (1992) [arXiv:hep-lat/9207009].

[19] M. Lüscher, R. Sommer, P. Weisz and U. Wolff, "A precise determination of the running coupling in the SU(3) Yang-Mills theory," Nucl. Phys. B **413**, 481 (1994) [arXiv:hep-lat/9309005].

[20] S. Sint, "On the Schrodinger functional in QCD," Nucl. Phys. B **421**, 135 (1994) [arXiv:hep-lat/9312079]; "One Loop Renormalization Of The QCD Schrodinger Functional," **451**, 416 (1995) [arXiv:hep-lat/9504005].

[21] S. Sint and R. Sommer, "The running coupling from the QCD Schrödinger functional: A one loop analysis," Nucl. Phys. B **465**, 71 (1996) [arXiv:hep-lat/9508012].

[22] K. Jansen and R. Sommer [ALPHA collaboration], "O(α) improvement of lattice QCD with two flavors of Wilson quarks," Nucl. Phys. B **530**, 185 (1998) [Erratum-*ibid.* B **643**, 517 (2002)] [arXiv:hep-lat/9803017].

[23] M. Della Morte *et al.* [ALPHA Collaboration], "Computation of the strong coupling in QCD with two dynamical flavours," Nucl. Phys. B **713**, 378 (2005) [arXiv:hep-lat/0411025].

[24] T. Appelquist, G. T. Fleming and E. T. Neil, "Lattice study of the conformal window in QCD-like theories," Phys. Rev. Lett. **100**, 171607 (2008) [Erratum-ibid. **102**, 149902 (2009)] [arXiv:0712.0609 [hep-ph]].

[25] T. Appelquist, G. T. Fleming and E. T. Neil, "Lattice Study of Conformal Behavior in SU(3) Yang-Mills Theories," Phys. Rev. D **79**, 076010 (2009) [arXiv:0901.3766 [hep-ph]].

[26] A. J. Hietanen, K. Rummukainen and K. Tuominen, "Evolution of the coupling constant in SU(2) lattice gauge theory with two adjoint fermions," Phys. Rev. D **80**, 094504 (2009) [arXiv:0904.0864 [hep-lat]].

[27] F. Bursa, L. Del Debbio, L. Keegan, C. Pica and T. Pickup, "Mass anomalous dimension in SU(2) with two adjoint fermions," Phys. Rev. D **81**, 014505 (2010)

[arXiv:0910.4535 [hep-ph]].
[28] F. Bursa, L. Del Debbio, L. Keegan, C. Pica and T. Pickup, "Mass anomalous dimension in SU(2) with six fundamental fermions," Phys. Lett. B **696**, 374 (2011) [arXiv:1007.3067 [hep-ph]].
[29] M. Hayakawa, K. -I. Ishikawa, Y. Osaki, S. Takeda, S. Uno and N. Yamada, "Running coupling constant of ten-flavor QCD with the Schrödinger functional method," Phys. Rev. D **83**, 074509 (2011) [arXiv:1011.2577 [hep-lat]].
[30] T. Karavirta, J. Rantaharju, K. Rummukainen and K. Tuominen, "Determining the conformal window: SU(2) gauge theory with $N_f = 4$, 6 and 10 fermion flavours," arXiv:1111.4104 [hep-lat].
[31] B. Sheikholeslami and R. Wohlert, "Improved continuum limit lattice action for QCD with Wilson fermions," Nucl. Phys. B **259**, 572 (1985).
[32] A. Hasenfratz and F. Knechtli, "Flavor symmetry and the static potential with hypercubic blocking," Phys. Rev. D **64**, 034504 (2001) [arXiv:hep-lat/0103029].
[33] A. Hasenfratz, R. Hoffmann and S. Schaefer, "Hypercubic smeared links for dynamical fermions," JHEP **0705**, 029 (2007) [arXiv:hep-lat/0702028].
[34] S. Sint and P. Weisz [ALPHA collaboration], "The running quark mass in the SF scheme and its two-loop anomalous dimension," Nucl. Phys. B **545**, 529 (1999) [arXiv:hep-lat/9808013].
[35] S. Capitani, M. Lüscher, R. Sommer and H. Wittig [ALPHA Collaboration], "Non-perturbative quark mass renormalization in quenched lattice QCD," Nucl. Phys. B **544**, 669 (1999) [arXiv:hep-lat/9810063].
[36] M. Della Morte *et al.* [ALPHA Collaboration], "Non-perturbative quark mass renormalization in two-flavor QCD," Nucl. Phys. B **729**, 117 (2005) [arXiv:hep-lat/0507035].
[37] W. E. Caswell, "Asymptotic behavior of nonabelian gauge theories to two loop order," Phys. Rev. Lett. **33**, 244 (1974).
[38] T. Banks and A. Zaks, "On the phase structure of vector-like gauge theories with massless fermions," Nucl. Phys. B **196**, 189 (1982).
[39] Y. Shamir, B. Svetitsky, E. Yurkovsky, "Improvement via hypercubic smearing in triplet and sextet QCD," Phys. Rev. **D83**, 097502 (2011). [arXiv:1012.2819 [hep-lat]].
[40] M. Hasenbusch, "Speeding up the Hybrid-Monte-Carlo algorithm for dynamical fermions," Phys. Lett. B **519**, 177 (2001) [arXiv:hep-lat/0107019].
[41] C. Urbach, K. Jansen, A. Shindler and U. Wenger, "HMC algorithm with multiple time scale integration and mass preconditioning," Comput. Phys. Commun. **174**, 87 (2006) [arXiv:hep-lat/0506011].
[42] T. Takaishi and P. de Forcrand, "Testing and tuning new symplectic integrators for hybrid Monte Carlo algorithm in lattice QCD," Phys. Rev. E **73**, 036706 (2006) [arXiv:hep-lat/0505020].
[43] Y. Iwasaki, K. Kanaya, S. Sakai and T. Yoshié, "Quark confinement and number of flavors in strong coupling lattice QCD," Phys. Rev. Lett. **69**, 21 (1992).
[44] Y. Iwasaki, K. Kanaya, S. Kaya, S. Sakai and T. Yoshié, "Phase structure of lattice QCD for general number of flavors," Phys. Rev. D **69**, 014507 (2004) [arXiv:hep-lat/0309159].
[45] K. Nagai, G. Carrillo-Ruiz, G. Koleva and R. Lewis, "Exploration of SU(N_c) gauge theory with many Wilson fermions at strong coupling," Phys. Rev. D **80**, 074508 (2009) [arXiv:0908.0166 [hep-lat]].
[46] P. de Forcrand, S. Kim and W. Unger, "Conformality in many-flavour lattice QCD at strong coupling," arXiv:1208.2148 [hep-lat].
[47] P. de Forcrand, S. Kim and W. Unger, "A surprise with many-flavor staggered fermions in the strong coupling limit," arXiv:1211.3374 [hep-lat].
[48] L. Del Debbio, M. T. Frandsen, H. Panagopoulos and F. Sannino, "Higher representations on the lattice: Perturbative studies," JHEP **0806**, 007 (2008) [arXiv:0802.0891 [hep-lat]].
[49] J. B. Kogut and D. K. Sinclair, "Thermodynamics of lattice QCD with 2 flavours of colour-sextet quarks: A model of walking/conformal Technicolor," Phys. Rev. D **81**, 114507 (2010) [arXiv:1002.2988 [hep-lat]].
[50] J. B. Kogut and D. K. Sinclair, "Thermodynamics of lattice QCD with 2 sextet quarks on N_t=8 lattices," Phys. Rev. D **84**, 074504 (2011) [arXiv:1105.3749 [hep-lat]].
[51] D. K. Sinclair and J. B. Kogut, "The chiral phase transition for QCD with sextet quarks," arXiv:1111.2319 [hep-lat].
[52] D. K. Sinclair and J. B. Kogut, "QCD with colour-sextet quarks," arXiv:1211.0712 [hep-lat].
[53] Z. Fodor, K. Holland, J. Kuti, D. Nógrádi and C. Schroeder, "Chiral symmetry breaking in fundamental and sextet fermion representations of SU(3) color," arXiv:1103.5998 [hep-lat].
[54] Z. Fodor, K. Holland, J. Kuti, D. Nogradi, C. Schroeder and C. H. Wong, "Twelve fundamental and two sextet fermion flavors," arXiv:1205.1878 [hep-lat].
[55] Z. Fodor, K. Holland, J. Kuti, D. Nogradi, C. Schroeder and C. H. Wong, "Can the nearly conformal sextet gauge model hide the Higgs impostor?," Phys. Lett. B **718**, 657 (2012) [arXiv:1209.0391 [hep-lat]].
[56] Z. Fodor, K. Holland, J. Kuti, D. Nogradi, C. Schroeder and C. H. Wong, "Confining force and running coupling with twelve fundamental and two sextet fermions," arXiv:1211.3548 [hep-lat].
[57] Z. Fodor, K. Holland, J. Kuti, D. Nogradi, C. Schroeder and C. H. Wong, "The sextet gauge model, light Higgs, and the dilaton," arXiv:1211.6164 [hep-lat].
[58] `http://www.physics.utah.edu/~detar/milc/`
[59] A. Hasenfratz, R. Hoffmann and S. Schaefer, "Low energy chiral constants from epsilon-regime simulations with improved Wilson fermions," Phys. Rev. D **78**, 054511 (2008) [arXiv:0806.4586 [hep-lat]].
[60] S. Sint and P. Vilaseca, "Lattice artefacts in the Schrödinger Functional coupling for strongly interacting theories," arXiv:1211.0411 [hep-lat].
[61] S. Sint and P. Vilaseca, "Perturbative lattice artefacts in the SF coupling for technicolor-inspired models," PoS LATTICE **2011**, 091 (2011) [arXiv:1111.2227 [hep-lat]].
[62] T. Karavirta, K. Tuominen and K. Rummukainen, "Perturbative Improvement of the Schrödinger Functional for Lattice Strong Dynamics," Phys. Rev. D **85**, 054506 (2012) [arXiv:1201.1883 [hep-lat]].
[63] T. Karavirta, K. Rummukainen and K. Tuominen, "Effect of the Schrödinger functional boundary conditions on the convergence of step scaling," arXiv:1210.0351 [hep-lat].